Electrochemical and Neutron Reflectivity Characterization of Dodecyl Sulfate Adsorption and Aggregation at the Gold−Water Interface

I. Burgess, V. Zamlynny, G. Szymanski, and J. Lipkowski*

Department of Chemistry and Biochemistry, University of Guelph, Guelph, Ontario N1G 2W1, Canada

J. Majewski and G. Smith

MLNSCE, LANSCE-12, Los Alamos National Laboratory, Los Alamos, New Mexico 87545

S. Satija and R. Ivkov

NIST Center for Neutron Research, NIST, Gaithersburg, Maryland

Received November 27, 2000. In Final Form: February 13, 2001

Chronocoulometry and the thermodynamic analysis of charge density data were employed to describe the energetics of sodium dodecyl sulfate (SDS) adsorption at the Au(111) electrode surface. Thermodynamic data such as the Gibbs excess, Gibbs energy of adsorption, and the film pressure of adsorbed SDS were determined for a broad range of electrode potentials, charge densities, and bulk SDS concentrations. The present results, combined with our previous scanning probe microscopy (SPM) studies, show that adsorption of SDS at the Au(111) electrode surface has a two-state character. At small or moderate absolute charge densities, the adsorbed SDS molecules aggregate into hemicylindrical stripelike micelles. This state is well-ordered. The unit cell of its two-dimensional lattice consists of two vectors that are 44 and 5.0 Å long and are oriented at an angle of 70°. The Gibbs excess data indicate that five SDS molecules are accommodated into the unit cell. At large positive charge densities, the hemimicellar aggregates melt to form a condensed film. The surface concentration of SDS doubles upon transition from the hemimicellar to the condensed state. We have performed neutron reflectivity experiments to determine the thickness of the hemimicellar and condensed films. The neutron reflectivity data indicate that the thickness of the condensed film is equal to 20.5 Å and is only 30% larger than the thickness of the hemimicellar state. The electrochemical and neutron reflectivity data indicate that the properties of the condensed state are best explained by a model of an interdigitated film in which half of the sulfate groups are turned toward the metal and half toward the solution.

Introduction

The objective of the present work is to complement the results of our previous SPM studies[1] with new information concerning the surface concentration of SDS as well as the thickness and compactness of the film that these molecules form at the Au(111) electrode surface. In the present paper we have employed electrochemical techniques to determine the Gibbs surface excesses (surface concentration) of adsorbed SDS molecules and neutron reflectivity (NR) measurements to obtain the density profile for the SDS covered gold electrode surface. The information concerning the film thickness and its compactness was extracted from the density profile. The results of this work, when combined with our earlier results, offer a complete description of the structure and composition of the SDS film at the Au(111) electrode surface. We present here a rigorous thermodynamic description of SDS adsorption at the Au(111)−solution interface. While, the adsorption of SDS on gold has attracted relatively little attention, the adsorption of SDS on mercury has been extensively studied by electrochemical techniques.[2−14] Wandlowski et al.[12] provided a thorough review of this literature. When appropriate we use information available in the literature to compare the behavior of SDS molecules at Au(111) and mercury electrode surfaces.

In our previous studies we reported scanning probe microscopy (SPM) and electrochemical measurements concerning the adsorption and aggregation of SDS at the Au(111) surface at concentrations greater than the critical micelle concentration (cmc). We have demonstrated that the adsorption of SDS has a two-state character. At small or moderate absolute charge densities, the adsorbed SDS molecules aggregate into hemicylindrical stripelike hemimicelles. When the charge is positive and the charge

(1) Burgess, I.; Jeffrey, C. A.; Cai, X.; Szymanski, G.; Galus, Z.; Lipkowski, J. *Langmuir* **1999**, *15*, 2607−2616.
(2) Eda, K. *Nippon Kagaku Zasshi* **1959**, *80*, 349.
(3) Eda, K. *Nippon Kagaku Zasshi* **1959**, *80*, 708.
(4) Foresti, M. L.; Moncelli, M. R. *J. Electroanal. Chem.* **1978**, *92*, 61.
(5) Damaskin, B. B.; Nikolaeva-Fedorovich, N. V.; Ivanova, R. V. *Zh. Fiz. Khim.* **1960**, *34*, 894.
(6) Kaisheva, M. K.; Gyrkov, T. D.; Damaskin, B. B. *Elekrokhimiya* **1985**, *21*, 832.
(7) Kaisheva, M. K.; Kaishev, V. K. *Elektrokhimiya* **1986**, *22*, 854.
(8) Trujillo, J. P.; Bennes, R. C. *R. Acad. Sci.* **1979**, *288C*, 355.
(9) Naficy, G.; Vanel, V.; Schuhmann, D.; Bennes, R.; Tromel-Peyroz, E. *J. Phys. Chem.* **1981**, *85*, 1037.
(10) Papadopoulos, N.; Sotiropoulos, S.; Nikitas, P. *J. Electroanal. Chem.* **1992**, *324*, 375.
(11) Sotiropoulos, S.; Nikitas, P.; Papadopoulos, N. *J. Electroanal. Chem.* **1993**, *356*, 201.
(12) Wandlowski, T.; Hromodova, M.; de Levie, R. *Langmuir* **1997**, *13*, 2766.
(13) Nikitas, P.; Sotiropoulos, S.; Papadopoulos, N. *J. Phys. Chem.* **1992**, *96*, 8453.
(14) Nikitas, P. *J. Electroanal. Chem.* **1993**, *348*, 59.

10.1021/la001628q CCC: $20.00
Published on Web 04/25/2001

density is large, the hemimicellar aggregates melt to form a condensed film.

The formation of hemimicellar aggregates was initially proposed by Fuerstenau.[15] Manne and co-workers[16] and Ducker and co-workers[17] provided the first AFM images of these aggregates of surfactant molecules on atomically flat surfaces. With the help of high-resolution STM images of the hemimicellar aggregates, we were able to reveal that the adsorbed SDS molecules are ordered, forming a long-range, two-dimensional lattice.[1] A unit cell of this lattice consists of two vectors that are 44 and 5.0 Å long and are oriented at an angle of 70°. We proposed that each unit cell contained two flat-lying SDS molecules stretched out along the longer axis of the cell with the hydrocarbon tails directed toward the interior of the cell. The remaining SDS molecules in the hemimicelle assume an orientation out of the plane of the electrode. This long-range structure is stabilized by the interactions of sulfate groups belonging to the adjacent cells. The sulfate groups of the flat-laying SDS molecules are arranged into a characteristic ($\sqrt{3} \times \sqrt{7}$) structure in which the sulfate groups along the $\sqrt{7}$ direction are bridged by hydrogen bonded water molecules.

Although our previous work offered direct visualization of both the hemimicellar and condensed phases and the phase transition between these two states, we were unable to determine the exact composition of either state. Specifically, we did not determine the number of monomer units comprising the cross-section of the hemimicelle nor were we able to describe the nature of the condensed film that formed after the charge-driven phase transition.

Experimental Section

To extract thermodynamic parameters pertaining to SDS adsorption on Au(111), it was necessary to work in solutions containing a supporting electrolyte (50 mM $KClO_4$) and at SDS concentrations below the cmc. From surface tension measurements, made using a Wilhelmy plate, the cmc for SDS in 50 mM $KClO_4$ was found to be ≈0.54 mM.

Materials. All solutions were prepared with Millipore (>18 MΩ) water. The $KClO_4$ (ACS Certified, Fisher) used to make the supporting electrolyte was purified using the method previously described.[18] The SDS was obtained commercially (Fluka, 99% pure) and twice recrystallized from ethanol to remove the dodecanol impurity. Freshly prepared solutions were used to minimize contamination from the slow hydrolysis of SDS.

Electrochemistry. The working electrode used in the electrochemical experiments was a massive, rod-shaped Au(111) single crystal. The electrode was flame-annealed, quenched with water, and introduced to a glass cell containing deaerated, supporting electrolyte (50 mM $KClO_4$). A flame-annealed, coiled gold wire served as the counter electrode. Ionic conductivity between the main cell and a second cell containing the saturated calomel reference electrode (SCE) was achieved with a salt bridge. The working electrode was employed in the hanging meniscus configuration to ensure that only the (111) face was in contact with the electrolyte. A PAR model 173 potentiostat and PAR model 5206 lock-in amplifier were interfaced with a personal computer via an RC Electronics data acquisition board. In-house software was used to collect the data for the cyclic voltammetry, (CV), differential capacity (DC), and chronocoulometry experiments. To record the differential capacity curves, a 25 Hz, 5 mV (rms), ac perturbation was superimposed on a 5 mV/s DC voltage sweep. The deaerated solution was kept under an argon blanket for the duration of the experiments. All measurements were carried out at a room temperature of 20 ± 2 °C. In aqueous solutions, the Krafft temperature of SDS is 16 °C[12] and no evidence of surfactant precipitation was observed for the experiments conducted at room temperature.

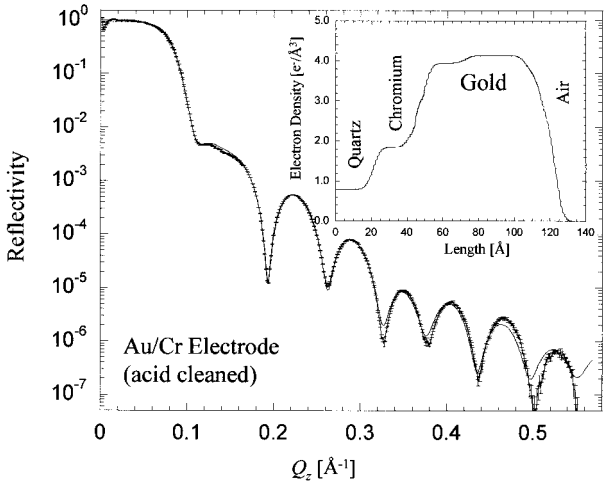

Figure 1. X-ray reflectivity curve measured in air for the Au/Cr modified quartz substrate used in the neutron reflectivity studies. The solid line represents the best fit to the data. The inset shows electron density versus length profile determined from the fitting procedure.

Neutron Reflectivity. Neutron reflectivity experiments were carried out on the NG-7 reflectometer at the National Institute of Standards and Technology (NIST) in Gaithersburg, MD. The working electrodes were derived from polished single-crystal quartz substrates obtained from CrysTec GmbH (Berlin, Germany). The root-mean-square roughness of the crystals was measured by X-ray reflectivity to be about 5 Å. Thin layers of chromium (∼20 Å) and gold (∼80 Å) were sequentially sputtered on the substrates. The cyclic voltammetry curves recorded on these thin film gold electrodes resembled CVs recorded at the Au(111) surface, suggesting that the sputtered gold layer was preferentially (111) oriented. The gold-coated crystals were degreased with ethanol, cleaned in warm (∼60 °C) concentrated sulfuric acid, and washed thoroughly with Milli-Q water (>18 MΩ).

The properties of the thin Au/Cr layers were characterized by X-ray and neutron scattering in air. The X-ray reflectivity data of the sputtered Au/Cr layers is shown in Figure 1. The solid line is the least-squares fit to the data using a box model and the resulting electron density profile is shown in the inset. The values of the fitting parameters are shown in Table 1. The fit was done with a model consisting of six boxes (one for Cr, one for the Au/Cr interface, and four to describe the electron density distribution in the gold layer. One rms roughness factor was used to smear the interfaces. The fit shows that the electrode structure can be approximately described by two boxes; a 22 Å thick Cr layer and an 80 Å thick layer of Au. These values match very well with the lengths we aimed for during the sputtering procedure. The electron densities of chromium and gold are slightly less than the theoretical values. The electron density of Cr is about 7% less than the theoretical value and the maximum electron density of the Au layer is 11% less than the value for the bulk gold. This

(15) (a) Gaudin, A. M.; Fuerstenau, D. W. *Trans. AIME* **1955**, *202*, 958. (b) Wakamatsu, T.; Fuerstenau, D.W. *Adv. Chem. Ser.* **1968**, *No.79*, 161. (c) Somasundaran, P.; Fuerstenau, D. W. *J. Phys. Chem.* **1966**, *70*, 70. (d) Fuerstenau, D. W.; Wakamatsu, T. *Faraday Discuss. Chem. Soc.* **1975**, *59*, 157.

(16) (a) Manne, S.; Cleveland, J. P.; Gaub, H. E.; Stucky, G. D.; Hansma, P. K. *Langmuir* **1994**, *10*, 4409. (b) Manne, S.; Gaub, H. E. *Science* **1995**, *270*, 1480. (c) Manne, S. *Prog. Colloid Polym. Sci.* **1997**, *103*, 226. (d) Manne, S.; Schaeffer, R.; Huo, Q.; Hansma, P. K.; Morse, D. E.; Stucky G. D.; Aksay, I. A. *Langmuir* **1997**, *13*, 6382. (e) Jaschke, M.; Butt, H.-J.; Gaub H. E.; Manne, S. *Langmuir* **1997**, *13*, 1381. (f) Patrick, H. N.; Warr, G. G.; Manne, S.; Ilhan, A. A. *Langmuir* **1997**, *13*, 4349. (g) Patrick, H. N.; Warr, G. G.; Manne, S.; Ilhan, A. A. *Langmuir* **1999**, *15*, 1685. (h) Wolgemuth, J. L.; Workman, R. K.; Manne, S. *Langmuir* **2000**, *16*, 3077.

(17) (a) Ducker, W. A.; Grant, L. M. *J. Phys. Chem.* **1996**, *100*, 11507. (b) Wanless, E. J.; Ducker, W. A. *J. Phys. Chem.* **1996**, *100*, 3207. (c) Wanless, E. J.; Ducker, W. A. *Langmuir* **1996**, *12*, 5915. (d) Wanless, E. J.; Ducker, W. A. *Langmuir* **1997**, *13*, 1463. (e) Wanless, E. J.; Davey, T. W. Ducker, W. A. *Langmuir* **1997**, *13*, 4223. (f) Lamont, R. E.; Ducker, W. A. *J. Am. Chem. Soc.* **1998**, *120*, 7602. (g) Liu, J. F.; Ducker, W. A. *J. Phys. Chem. B* **1999**, *103*, 8558. (h) Ducker, W. A.; Wanless, E. J. *Langmuir* **1999**, *15*, 160.

(18) Richer, J.; Lipkowski, J. *J. Electrochem. Soc.* **1986**, *133*, 121.

Table 1. Best-Fit Parameters for the Modified Quartz Substrate (Working Electrode) Determined from X-ray Reflectivity Measurements Made in Air[a]

Cr layer		Au/Cr layer		Au layers			
e-den, $e^-/Å^3$	T, Å	e-den, $e^-/Å^3$	T, Å	e-den, $e^-/Å^3$	T, Å	roughness σ Å	χ^2
1.85	21.7	2.82	6.95	3.94	22.5	3.3	67
(0.03)	(0.3)	(0.02)	(0.06)	(0.01)	(0.2)		
				4.13	34.4		
				(0.01)	(0.2)		
				3.71	8.2		
				(0.02)	(0.2)		
				2.50	8.3		
				(0.02)	(0.1)		
thickness: 21.7 Å				total Au thickness: 80.35 Å			

[a] e-den = electron density. Electron density of the monocrystalline quartz: 0.796 $e^-/Å^3$. Calculated electron density of bulk gold: 4.66 $e^-/Å^3$. Calculated electron density of bulk chromium: 2.0 $e^-/Å^3$.

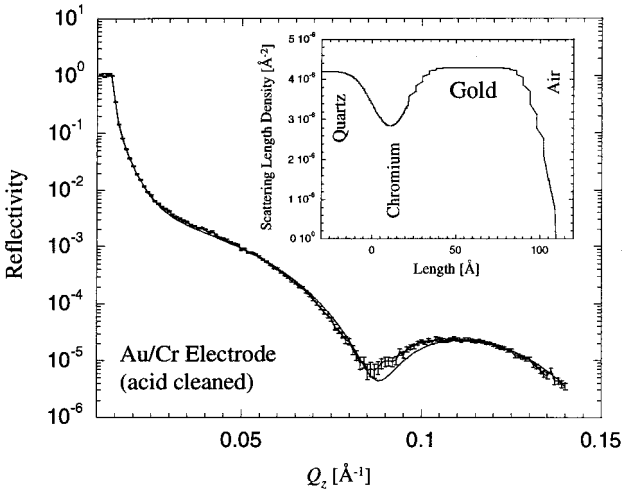

Figure 2. Neutron reflectivity curve measured in air for the Au/Cr modified quartz substrate used in the neutron reflectivity studies of SDS adsorption from aqueous media. The solid line represents the best fit to the data. Inset shows scattering length density versus length profile determined from the fitting procedure.

Table 2. Best-Fit Parameters for the Modified Quartz Substrate (Working Electrode) Determined from Neutron Reflectivity Measurements Made in Air[a]

Cr layer		Au layer			
scattering length density, 10^{-6} Å^{-2}	thickness, Å	scattering length density, 10^{-6} Å^{-2}	thickness, Å	roughness σ Å	χ^2
2.58	22.0	4.30	80.0	8.0	4.9
(0.02)	(fixed)	(0.02)	(fixed)	(0.1)	

[a] Scattering length density of the monocrystalline quartz: 4.2×10^{-6} Å^{-2}. Calculated scattering length density of bulk gold: 4.67×10^{-6} Å^{-2}. Calculated scattering length density of bulk chromium: 3.02×10^{-6} Å^{-2}.

means that the structure is "spongy", possibly due to cracks and voids in the layers.

The same crystal was also investigated using neutron reflectivity in air. The reflectivity data are shown in Figure 2. The solid line is the least-squares fit to the data using the box model and the resulting scattering length density profile is shown in the inset. The fit parameters are summarized in Table 2. The lengths of the Cr and Au boxes were fixed to the values obtained from the X-ray scattering. Consistent with the X-ray reflectivity data, the scattering length densities for Cr and Au are somewhat smaller than the theoretical values for the bulk metals (−14% for Cr and −8% for Au). These numbers indicate that the thin films of the two metals are not perfect. We will take these properties into account in the interpretation of the reflectivity data for the SDS covered electrode.

After cleaning, the crystal was mounted on a specially constructed Teflon cell, described in detail elsewhere.[19] The cell had ports for the counter (gold foil) and reference electrodes (Ag/AgCl, $E \sim -40$ mV versus SCE). The contact between the gold coated surface of the quartz substrate (working electrode) and a lead to the potentiostat was achieved by using a spring loaded steel bar. The resistance of the thin film of gold was on the order of a few ohms. D_2O (99.9%) from Sigma (St. Louis, MO) was used as a solvent in reflectivity studies. The cell was flushed with argon for 20 min before being filled with deaerated, D_2O solutions of SDS and 50 mM $KClO_4$. The experiments were carried out at a room temperature 20 ± 2 °C.

Neutron reflectivity measures the normalized (by the incident flux) intensity of specularly reflected neutrons R as a function of the momentum transfer vector Q_z ($Q_z = 4\pi \sin\theta/\lambda$, where θ is the angle of incidence and λ is the wavelength of the neutrons. A fixed neutron wavelength of 4.75 Å was used. Varying the angle of incidence allowed reflectivities to be measured in the Q_z range of ~0.0 to about 0.20 Å^{-1}. Reflectivities, R, with reasonable statistics were measured down to values of $R \sim 10^{-5}$. Typical counting times were 6−7 h. The reflected neutrons were counted using a ^{3}He detector. The data were reduced taking into account the neutron beam transmission through the quartz substrate and corrected for the background. The error points on the data represent the statistical errors in the measurements (standard deviation, σ_R). A constant instrumental resolution of $\Delta Q_z/Q_z = 0.043$ (fwhm) was used throughout the scan. An "inverted" geometry, in which the gold-coated quartz electrode was above the D_2O phase, was used in our experiments. In this case, the lower medium (D_2O) had a higher scattering length density than the upper one. Under these conditions the reflectivity was approximately unity for Q_z below a critical value $Q_c = 4(\pi\Delta\beta)^{1/2}$, where $\Delta\beta$ is the scattering length density difference between the lower and the upper media. Above Q_c, R decays as a function of Q_z and the character of this decay depends on the area-averaged scattering length density profile normal to the interface.

Results and Discussion

Differential Capacity. Differential capacity was used to qualitatively characterize the electrochemical behavior of the system. Figure 3a shows differential capacity curves recorded for a 0.33 mM SDS in 50 mM $KClO_4$ solution (top panel). The capacity curve for a pure solution of 50 mM $KClO_4$ is included for comparative purposes. The data in Figure 3a cover the potentials of the double-layer region of the gold electrode where the metal−solution interface behaves as a capacitor. The differential capacity curve for SDS displays features characteristic of two-state adsorption. At the most negative potentials, the differential capacity curve for SDS merges with the curve recorded for the inert electrolyte and this feature indicates that the surfactant is desorbed from the electrode surface. Moving from left to right in Figure 3a, two peaks are observed that are separated by a long relatively flat section

(19) Zamlynny, V.; Burgess, I.; Szymanski, G.; Lipkowski, J.; Majewski, J.; Smith, G.; Satija, S.; Ivkov, R. *Langmuir* **2000**, *16*, 9861.

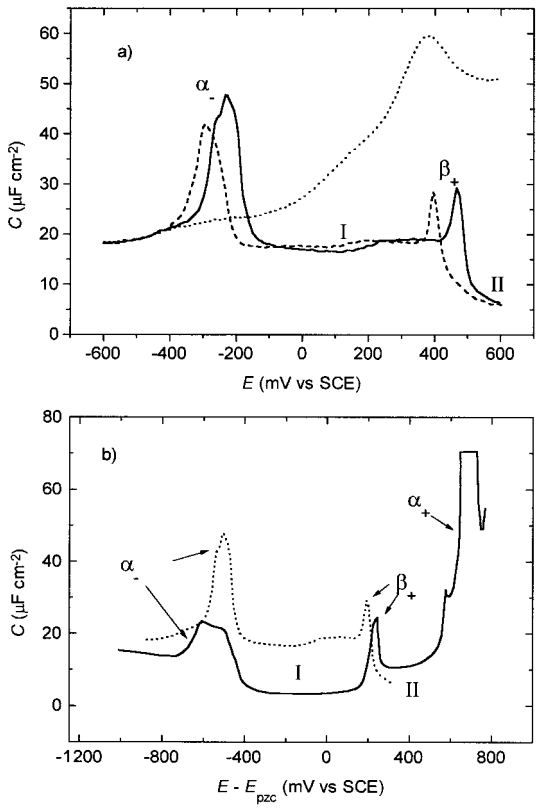

Figure 3. (a) Differential capacity curves recorded for a Au(111) electrode in a 50 mM $KClO_4$/0.33 mM (sub-cmc) solution of SDS, (—) positive going scan, (---) negative going scan, and (•••) 0.05 M $KClO_4$ electrolyte only. (b) Comparison of the differential capacity curves measured for a Au(111) electrode (•••) and for a dropping mercury electrode (—). The curve for the Au(111) electrode is from panel a obtained using a 25 Hz, 5 mV rms AC perturbation with a 5 mV/s DC potential sweep. The curve for the mercury electrode was recorded in a 0.16 M Na_2SO_4/0.5 mM SDS solution using 120 Hz, 5 mV (peak-to-peak) AC modulation.[11] Both systems correspond to SDS concentrations 0.6 cmc.

(approximately $-200 < E < 200$ mV), in which the capacity assumes a value of $\sim 15\ \mu F\ cm^{-2}$. This region is labeled as state I. We have demonstrated in our previous work that it corresponds to the hemimicellar state.[1] At the positive limit of potentials (at $E > 500$mV), the capacity drops to a very low value $\sim 5\ \mu F\ cm^{-2}$. This section is denoted as state II of the SDS adsorption. Our previous AFM studies showed that it corresponds to the condensed state of the film.[1] The most negative peak corresponds to the adsorption/desorption of SDS and the second peak to a phase transition between states I and II of the adsorbed surfactant. The peaks are denoted as α_- and β_+, respectively.

The negative going DC scan shown in Figure 3a exhibits a large hysteresis over the entire range of potentials. Such a hysteresis implies that the state of the adsorbed surfactant is dependent on the kinetics of the mass transport, adsorption/desorption, and phase transition processes. One can estimate the time needed to establish adsorption equilibrium from Koryta's equation[20]

$$t = \frac{1.85 \times 10^6}{D}\left(\frac{\Gamma}{c_i}\right)^2 \qquad (1)$$

where Γ is the amount of surfactant corresponding to a complete monolayer, D is the diffusion coefficient, and c_i is the surfactant concentration at infinite distance from the electrode, i.e., the bulk of the solution. For the highest SDS concentrations used in these experiments and assuming a diffusion coefficient on the order of 5×10^{-6} cm^2/s,[11] the time required for 4×10^{-10} mol/cm^2 (see below) to diffuse to the electrode surface is only $\approx$0.5 s. Thus the hysteresis exhibited in Figure 3a must be attributed to slow phase transition and adsorption/desorption processes.

The differential capacity curves for the SDS concentrations below the cmc shown in Figure 3a are quite similar to the curves shown in Figure 2a of ref 1 for SDS concentrations above the cmc. The only major differences are the size of the pseudo-capacitive peaks and the potential range corresponding to states I and II of the film. Such similarity implies that there are no major differences between the character of SDS adsorption at the Au(111) surface when the surfactant concentration is either lower or higher than the cmc. In addition, the character of SDS adsorption is not changed by the presence of supporting electrolyte.

Figure 3b compares the differential capacity curve for SDS adsorption at the Au(111) to the differential capacity curve recorded on a Hg electrode.[11] For the purpose of comparison, a rational potential scale is used in this figure. The data show that peaks α_- and β_+ appear at comparable rational potentials. However, the values of the differential capacity at potentials of state I are lower and in region II are higher at Hg than at the Au(111) electrode. In contrast to the Au(111) surface, at Hg it has been postulated that the condensed film is formed in region I and hemimicelles are formed in region II.[2,11,12] No direct evidence for the formation of hemimicelles at the Hg interface has been provided. Nevertheless, the character of SDS adsorption depends on the nature of the metal.

Chronocoulometry. Chronocoulometry was used to describe SDS adsorption at the Au(111) electrode surface quantitatively. The range of SDS concentrations studied in this work spanned from 0.01 to 0.33 mM. At concentrations lower than 10^{-5} M, the time required to reach adsorption equilibrium is unreasonably large. Charge densities were measured by waiting at potentials corresponding to SDS adsorption sufficiently long to ensure the establishment of adsorption equilibrium. Such waiting times were as long as 3 min, during which time the solution was stirred to ensure a high rate of mass transport. The stirring was turned off, allowing the solution to return to a quiescent state, before the current transient was measured.

Figure 4 shows the measured charge densities for various concentrations of SDS. It is convenient to discuss the charge density curves by dividing them into three regions, corresponding to states of complete desorption ($E < -350$ mV), hemimicelles (state I), and a condensed film (state II). Separating these regions are potentials where the charge density on the metal side of the interface increases sharply. These are attributed to the adsorption of SDS and the subsequent phase transition at more positive potentials. As the concentration of SDS in the bulk of the solution increases, both points of inflection shift in the negative direction.

The coordinates where the charge density curve for a given SDS solution intersects the curve for the supporting electrolyte provide both the potential (E_M) and charge ($\sigma_{m,M}$) where adsorption maxima or minima occur. It is evident from Figure 4 that the number of points of intersection depends on the SDS concentration. Moving in a positive direction, there is an initial point of intersection for all SDS curves at $E_{M1} \approx 340$ mV with a corresponding $\sigma_{m,M1}$ value of $\approx 6\ \mu C/cm^2$. This number is quite close to the value of $\sigma_m \approx 2\ \mu C/cm^2$ reported for the

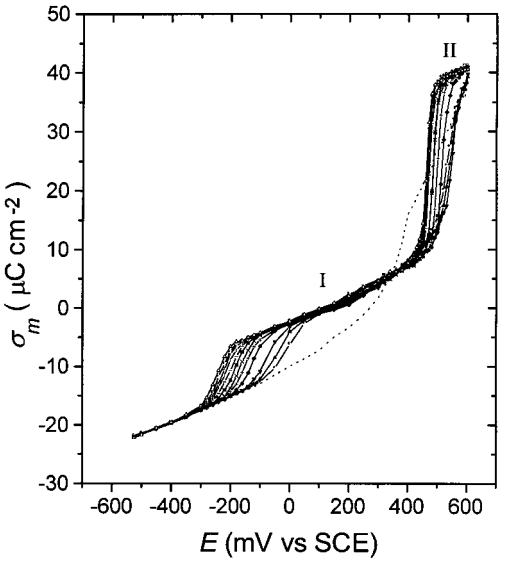

Figure 4. Charge density versus electrode potential data for solutions of SDS in 0.05 M $KClO_4$ in contact with a Au(111) electrode. The concentrations of SDS were (---) 0 mM; (●) 0.006 mM; (▲) 0.01 mM; (▼) 0.02 mM; (◆) 0.06 mM; (+) 0.09 mM; (•) 0.12 mM; (*) 0.16 mM; (−) 0.19 mM; (|) 0.23 mM; (□) 0.26 mM; (○) 0.29 mM; (△) 0.33 mM.

mercury electrode.[9] The charge density curves for low SDS concentrations (i.e., ≤0.02 mM) do not intersect the electrolyte curve again but rather become convergent with the pure electrolyte curve when E is larger than +575 mV. Interestingly, when the SDS concentration is increased to 0.06 mM the curves do intersect again at $E_{M2} = 525$ mV, $\sigma_m = 29\,\mu$C/cm^2. This second point of intersection strongly depends on the surfactant concentration, shifting negatively in potential by 60 mV and decreasing in charge density by 7 μC/cm^2 over the range of concentrations studied. We will show later that this second point of intersection corresponds to the minimum on the film pressure versus potential (or versus charge) curve, indicating a transition from the hemimicellar to the condensed state of the film.

The chronocoulometric data allow for the determination of the shift in the potential of zero charge, E_N. In the absence of SDS, the potential of zero charge for Au(111) in 50 mM $KClO_4$ is 275 mV vs SCE. From Figure 4, the charge density curve for the lowest concentration of SDS intersects the zero line of the ordinate axis at a potential of 150 mV. This point of intersection occurs in the range of potentials corresponding to state I and gives a value of E_N(state I) = −0.125 V. Although the charge density curves corresponding to state II of the SDS adsorption do not cross the zero charge line, the potential of zero charge can be determined from extrapolation. When a line with a slope 5 μF cm^{-2} (the value of the differential capacity for state II) is carried through charge densities for state II and extrapolated to zero charge density, one obtains a value of E_N (state II) equal to −7.8 V. The shift of E_{pzc} may be discussed in terms of three contributions; (1) the potential generated by the specifically adsorbed anions,[21] (2) the potential drop across the diffuse layer, ϕ_2, and (3) a change of potential due to the displacement of N_w water dipoles by the adsorbed SDS ions. Combining these contributions, E_N may be expressed as[22]

$$E_N = \frac{zF\Gamma(x_2 - x_1)}{\epsilon} + \phi_2 - \frac{N_w\bar{\mu}_w}{\epsilon} \qquad (2)$$

where ϵ is the dielectric permittivity of the inner layer, Γ is the Gibbs excess of adsorbed anion, z is the charge of an SDS molecule, and $\bar{\mu}_w$ is the average dipole moment, in the direction normal to the surface, of the water molecules on the electrode surface. The distance between the electrode and the specifically adsorbed anion (i.e., the $-OSO_3^-$ headgroup) is x_1, whereas the plane of closest approach for the solvated electrolyte ions to the surfactant covered electrode is defined to be x_2. For the adsorption of anions, the first two terms in eq 2 should be negative. At the pzc, water molecules at the gold electrode surface are expected to display a weak preferential orientation in which the oxygen atom is turned toward the metal surface. For this orientation, the averaged dipole $\bar{\mu}_w$ should be negative. Therefore, the third term is expected to bring a small positive contribution to ΔE_{pzc}. The negative sign of the measured values of ΔE_{pzc} indicates that the first two terms dominate. The small absolute value of ΔE_{pzc} for the hemimicellar state of the film suggests that $(x_2 - x_1)$ is small. This behavior indicates that in the hemimicellar state, SDS molecules are oriented with the hydrocarbon tail directed to the electrode and the polar head turned to the solution. In contrast, the large absolute value of ΔE_{pzc} for the condensed film suggests that $(x_2 - x_1)$ is large. Therefore, in the condensed film, dodecyl sulfate headgroups are adjacent to the electrode surface and the hydrocarbon tails are turned to the solution.

We will later consider a model of a condensed phase in which approximately half of surfactant molecules are turned with sulfate groups to the metal and another half toward the solution. The shift of pzc for this model is described by

$$E_N = \frac{zF\,\Gamma^d(x_2 - x_1{}^d)}{\epsilon} + \frac{zF\Gamma^u(x_2 - x_1{}^u)}{\epsilon} + \phi_2 - \frac{N_w\bar{\mu}_w}{\epsilon} \qquad (3)$$

where superscripts d and u refer to surfactant molecules turned "down" toward the metal and "up" toward the solution, respectively. The first term in eq 3 will dominate and hence for the model of interdigitated surfactant molecules a significant shift of the pzc in the negative direction should also be observed by moving from the hemimicellar to the condensed state of the film.

There is confusion concerning the value of ΔE_{pzc} for SDS on mercury.[7] The only value reported in the literature comes from the paper by Kaisheva and Kaishev.[7] Unfortunately, these authors reported a positive ΔE_{pzc} in a table and a negative value in the text.

Surface Pressure. Integration of the charge density vs electrode potential data was used to calculate the film pressure as a function of SDS concentration. In addition, the Parsons function $\xi = \gamma + \sigma_M E$ was calculated and the surface pressures at constant charge $\phi = \xi_{c=0} - \xi_c$ were determined as a function of the charge density on the electrode.

The π versus E and ϕ versus σ_m plots are shown in parts a and b of Figure 5, respectively. In the region of the electric variable corresponding to state I, all curves display a bell-shaped appearance with a distinct maximum at the point of maximum adsorption, $E_{m,M1}$. This corresponds to a potential of +340 mV for the π versus E curve and an electrode charge density of +6 μC/cm^2 for the ϕ versus σ_M curve. These values correspond well to the charge and potential at which the charge density curves for SDS solutions intersect the curve for the supporting electrolyte.

(20) Koryta, J. *Collect. Czech Commun.* **1953**, *18*, 206.
(21) Grahame, D. C. *Z. Elektrochem.* **1958**, *62*, 264.
(22) Payne, R. *Trans. Faraday Soc.***1968**, *64*, 1638.

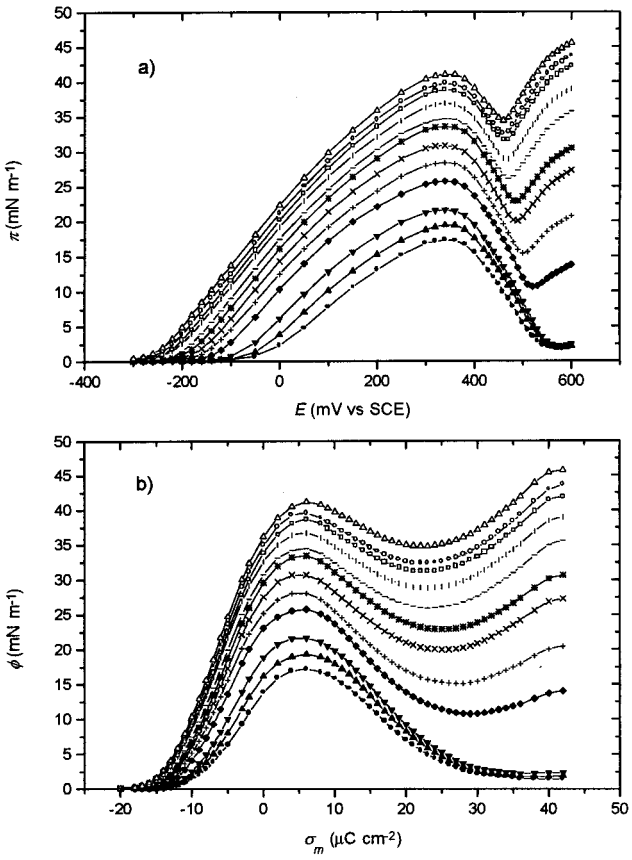

Figure 5. (a) Surface pressure versus electrode potential and (b) surface pressure versus electrode charge density curves obtained from integration of the charge density data for the following SDS concentrations; (b) 0.006 mM; (▲) 0.01 mM; (▼) 0.02 mM; (◆) 0.06 mM; (+) 0.09 mM; (●) 0.12 mM; (∗) 0.16 mM; (−) 0.19 mM; (|) 0.23 mM; (□) 0.26 mM; (○) 0.29 mM; (△) 0.33 mM.

The surface pressure curves are highly dependent on the SDS concentration at potentials and charges corresponding to state II. For SDS concentrations ≤0.02 mM, both the surface and film pressures approach zero for large positive electrode polarizations, indicating desorption of the surfactant film. As the concentration increases, the surface pressure plots display a bimodal appearance with a distinct minimum at $E_{m,M2}$ (or $\sigma_{m,M2}$ in the case of Figure 5b). The surface pressure data can be explained as arising from the superposition of two bell-shaped curves corresponding to the two different orientations of the adsorbed molecules. The minimum in the pressure curves corresponds to the second point at which the charge density curves for the SDS solutions intersect the curve for the supporting electrolyte. As mentioned earlier it indicates the point of the phase transition between the adsorbed states. Its shift toward more negative potentials indicates that the formation of state II becomes more energetically favorable on the surface as the SDS concentration increases.

Adsorption Isotherms. Determination of the relative Gibbs surface excess is achieved via differentiation of the film pressure versus the logarithm of the bulk SDS concentration curves. Presented in Figure 6a are the Γ values determined by using *E* as the independent electrical variable. The Gibbs excesses determined using charge as the independent variable are plotted in Figure 6b. The graphs are three-dimensional (3-D). The surface concentrations are plotted along the vertical axis, while the electrode potential (or the charge density at the metal)

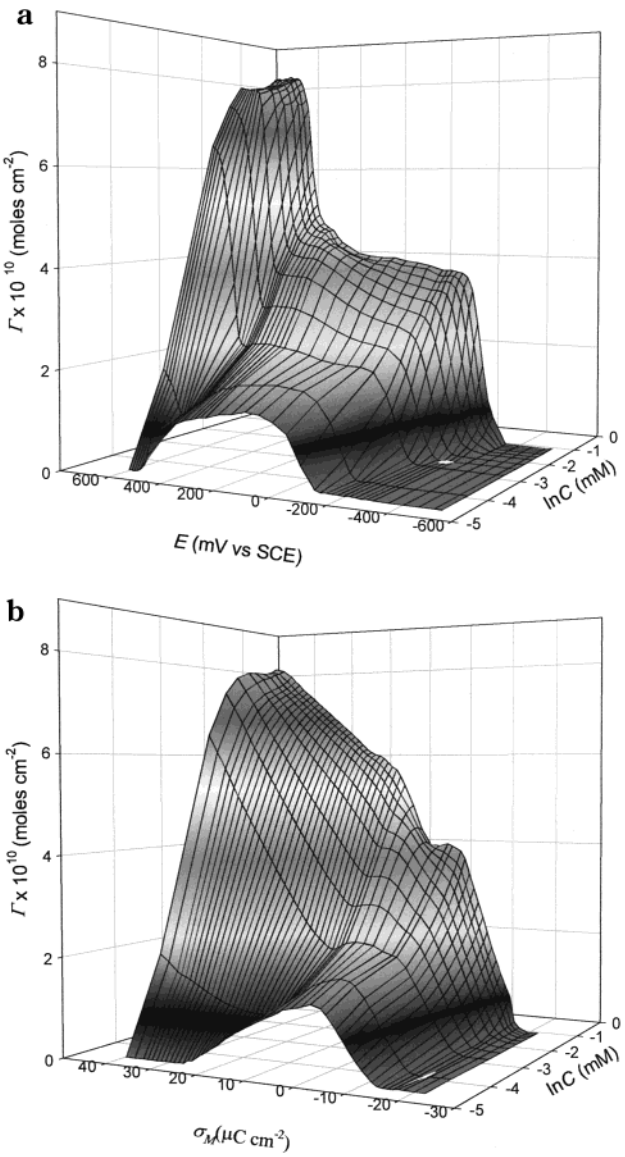

Figure 6. Three-dimensional plots of the Gibbs surface excess of SDS as a function of (a) electrode potential and the logarithm of the bulk SDS concentration and (b) electrode charge density and the logarithm of the bulk SDS concentration.

and the logarithm of the bulk SDS concentration are plotted as the basal plane. When the bulk SDS is small (less than 5×10^{-5} M) the adsorption of SDS has a one-state character. Here, the Γ versus *E* (or versus σ_M) curves at a constant bulk concentration are bell shaped with the maximum appearing close to the pzc (at small charge densities). At higher SDS concentrations the 3-D graphs display two well-defined plateaus, the first appearing at potentials corresponding to state I of SDS adsorption. The limiting surface excess in the first plateau is 4.0×10^{-10} mol cm^{-2}. This value can be compared to the surface concentration of SDS on graphite determined by Greenwood et al.[23] to be 3.7×10^{-10} mol/cm^2, in the absence of supporting electrolyte. The present result for Au(111) and Greenwood's result for graphite agree within the limits of the experimental error. The surface concentrations for gold and graphite are higher than the Gibbs excess for a monolayer of SDS molecules at the air−solution interface

(23) Greenwood, F. G.; Parfitt, G. D.; Picton, N. H.; Wharton, D. G. In *Adsorption from Aqueous Solution*; Weber, W. J., Matijevic, E., Eds.; American Chemical Society: Washington, DC, 1968; pp 135−144.

equal to 3.3×10^{-10} mol/cm^2 (ref 24) or at mercury−solution interface equal to 2.8×10^{-10} mol/cm^2.[8,9]

The second plateau is observed at potentials positive of the phase transition and corresponds to a limiting surface concentration of 8.1×10^{-10} mol/cm^2. Thus, the phase transition corresponds to a doubling of the number of molecules in the interfacial region. From the shift in the potential of zero charge data it is evident that the phase transition is consistent with the formation of a film of surfactant molecules with their negatively charged headgroups directed toward the metal surface. It is also apparent that the phase transition occurs when the electrode incurs a large, positive charge density. It is likely that this positive charge on the metal surface screens the electrostatic repulsion between the surfactant headgroups, allowing for a much greater packing density.

It is useful to note that when E is used as the independent electrical variable (Figure 6a) the transition from the hemimicellar to the condensed state of the film is very sharp. However, with charge as the electrical variable, the transition appears much more gradual. Although the shapes of the adsorption isotherms are different, comparison of part a and b of Figure 6 reveals that the limiting Gibbs surface excesses for the two adsorption states are independent of the choice of electrical variable. Figure 6a,b also shows that although the region of potentials corresponding to the hemimicellar state is very broad, this state exists in a narrow range of very small charge densities (in the vicinity of the zero charge).

Gibbs Energy of Adsorption. The standard Gibbs energies of adsorption, ΔG^0_{ads}, were determined from the initial slopes of surface pressure versus mole fraction of SDS plots using the expression for Henry's Law isotherm.

$$\pi = RT\Gamma^*_{max}\beta\frac{c}{55.5} \tag{4}$$

The standard state was defined as being unit mole fraction of SDS in the bulk and a monolayer coverage of "ideal" noninteracting SDS molecules at the surface. In calculating ΔG^0_{ads}, the maximum surface coverage observed in the region of polarizations corresponding to state I (4.0×10^{-10} mol/cm^2) was used for Γ_{max}.

Figure 7a,b shows separate plots of ΔG^0_{ads} versus electrode potential and charge density. The Henry isotherm could only be applied for low surface pressures corresponding to electrode potentials and charge densities below 100 mV and 0 μC/cm^2, respectively. The standard free energies, calculated in this manner, reach a minimum value of -39 ± 1 kJ/mol, suggesting that the SDS is weakly chemisorbed to the Au(111) substrate.

The almost discontinuous change of surface concentration at the phase transition prevents direct determination of the zero coverage Gibbs energy of adsorption. However, the energetics can be quantified in terms of full coverage Gibbs energies of adsorption, $\Delta G^{0,\theta=1}{}_{ads}$. The values of $\Delta G^{0,\theta=1}{}_{ads}$ can be obtained by plotting π versus ln(c/55.5) and extrapolating the linear portion of the plot back to zero surface pressure.[25] Multiplying the ln(c/55.5) intercept by RT gives the full coverage energy of adsorption. These values, as a function of electrode potential or charge density, are also shown in Figure 7a,b. Obviously, these data could only be obtained for electrical variables corresponding to full adsorbate coverage. Both curves display a minimum value of $\Delta G^{0,\theta=1}{}_{ads}$ in the region of

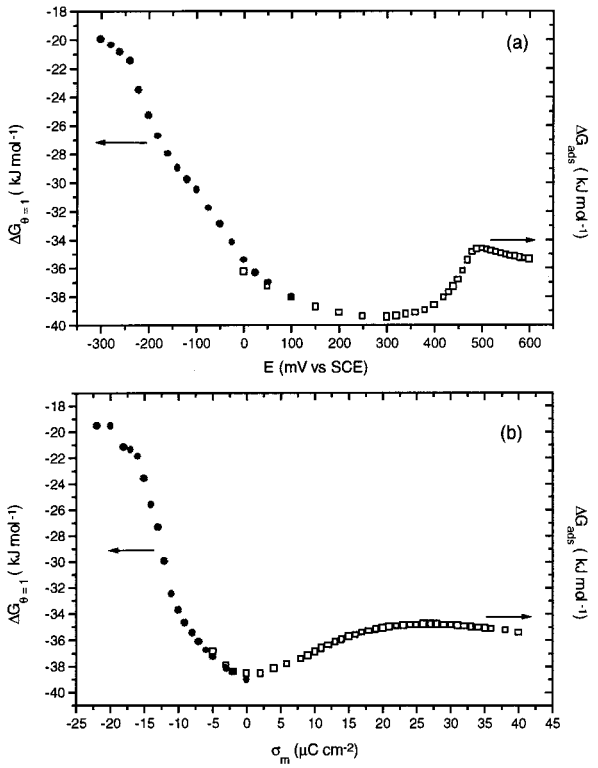

Figure 7. (a) Standard (zero-coverage) Gibbs energies of adsorption (●) for SDS on Au(111) as determined from application of the Henry's Law isotherm and full coverage Gibbs energy of adsorption (□) as a function of electrode potential. (b) The same plot as in panel (a) but with electrode charge density as the electrical variable.

state I. In Figure 7a, the minimum occurs at $E = 300$ mV, a potential very close to the E_{pzc} for a bare Au(111) electrode. This observation is reinforced by Figure 7b, which shows that the minimum full coverage Gibbs energy of absorption occurs in the vicinity of zero charge density.

Assuming a generalized adsorption isotherm, the relationship between $\Delta G^{0,\theta=1}{}_{ads}$ and ΔG^0_{ads} is given by eq 5:[25]

$$\Delta G^{0,\theta=1}ads = \Delta G^0 ads + RT \ln n + RT[na - (n-1)] \tag{5}$$

where n is the number of solvent molecules displaced from the electrode surface by one adsorbed SDS molecule and a is the lateral interaction constant. For nonideal adsorbates ($n \neq 1$, $a \neq 0$) there is a difference between $\Delta G^{0,\theta=1}{}_{ads}$ and ΔG^0_{ads}. Figure 7a,b shows that the full-coverage Gibbs energies of adsorption and those determined from the Henry isotherm are almost identical at overlapping electrode potentials and charge densities. This implies that a is positive (repulsive interaction) and that there is a significant cancellation of positive (na + ln n) and negative (n −1) terms.

Neutron Reflectivity. Neutron reflectivity measurements were performed in order to characterize the structure of the film of SDS molecules formed at different electrode potentials. Neutron reflectivity data allow one to determine the scattering length profile perpendicular to the electrode surface. The film thickness and the surface occupancy of the hydrogenated species may be calculated from the scattering length density profile. The information concerning the thickness of the film is particularly useful in determining whether SDS adsorption leads to the

(24) Sasaki, T.; Hattori, M.; Sasaki, J.; Nukina, K. *Bull. Chem. Soc. Jpn.* **1975**, *48*, 1397.
(25) Yang, D. F.; Stolberg, L.; Lipkowski, J.; Irish, D. E. *J. Electroanal. Chem.* **1992**, *329*, 259.

formation of a monolayer or a bilayer. Specifically, the electrochemical data discussed above demonstrated that the transition from the hemimicellar to the condensed state of the film is accompanied by a 2-fold increase in the surface concentration of SDS. This number suggests that the phase transition may correspond to a transformation of a monolayer into a bilayer. If this is the case, a significant change of the film thickness should take place upon the phase transition. Neutron reflectivity is ideally suited to detect the film thickness change. In addition, the information concerning the surface occupancy by the hydrogenated species provides unique insight into the compactness of the film and its penetration by the solvent. We have performed two series of measurements during two separate runs using two independently prepared crystals. In the first series, we investigated 16 and 0.5 mM SDS solutions corresponding to concentrations above and just below the cmc, respectively. In addition, the 16 mM SDS solution did not contain any supporting electrolyte, whereas the 0.5 mM solution contained 50 mM $KClO_4$. The second series of measurements were carried out in 0.3 mM SDS plus 50 mM $KClO_4$ solution using a crystal that was characterized using X-ray and neutron reflectivity measurements in air as described in the Experimental Section. We start the discussion from this series of measurements.

The reflectivity measurements in the presence of SDS were performed for three electrode potentials corresponding to the desorbed state ($E = -500$ mV), hemimicellar state ($E = 300$ mV), and condensed state ($E = 600$ mV). Figure 8a−c shows the neutron reflectivity curves collected at these potentials. The value of the momentum transfer vector was varied up to a value of 0.2 $Å^{-1}$, at which point the reflectivites approached the level of the background $R \sim 3 \times 10^{-6}$. This background occurs because of incoherent and thermal diffuse scattering from the solution of SDS in D_2O and the cell. At concentrations above the cmc, scatter from the micelles also contributes to the background. The reflectivity systematically increased with increasing potential by moving from the desorbed to the condensed state of the film. To extract structural information from these data, the reflectivities were analyzed using the iterative, dynamic method. The scattering length densities of chromium, gold, and the organic layers were modeled as boxes of a specified thickness and one overall root-mean-square roughness factor, σ, was used to smear out all the interfaces. Based on known facts about the system (thickness of the gold and chromium layers and possible structure of the organic layer at the interface), a model reflectivity profile was generated and compared to the measured reflectivity profile. The agreement of the calculated and the experimental curves was good for reflectivities greater than $R \sim 5 \times 10^{-6}$. The model was then minimized with the Marquardt-Levenburg nonlinear least-squares fitting routine in order to obtain the best least-squares fit to the data and the most physically reasonable parameters.

Our philosophy was to use the simplest yet most physically reasonable model to fit the experimental data. We began with simple one or two box models to account for the Cr and Au layers. If the simple model gave a large χ^2 value, we began to increase its complexity by adding boxes to account for various layers of the interfacial film. The results that are presented are the best fits to the data using simple, insightful models. Large variations in the parameter space were allowed, but we restricted our models to those that generated reasonable results based on the known lengths and scattering length densities of the constituent molecules. This enabled us to fit the data with a high level of self-consistency. Solid lines in Figure 8a−c show the best fits to the experimental data. The best-fit model of the scattering length density versus the distance in the direction normal to the surface is shown in Figure 8d. We note that for the hemimicellar state the SLD profile in the direction normal to the surface should be parabolic. Therefore, we have made an attempt to fit the data for $E = 300$ mV using a parabola instead of a rectangular box. Unfortunately, because the range of the momentum transfer vector Q was restricted to 0.2 $Å^{-1}$ and the roughness of the film was large (6.3 Å), the fit was not sensitive to the change of the SLD profile.

The parameters from these fits are summarized in Table 3. The thickness of the Cr and Au layers, taken from X-ray and neutron scattering experiments in air (Figures 1 and 2 and Tables 1 and 2), were kept constant during all the calculations. Small increases of the scattering lengths densities of the Au and Cr as compared to the values obtained for measurements in air can be explained by the D_2O-based electrolyte penetrating into these layers. The SLD values reported in Table 3 correspond to the heights of the box used to model the interface. The SLD values plotted in the figures are smeared out by convoluting the box with a Gaussian roughness characterized by the parameter σ in Table 3. For this reason, in Figure 8, the lowest scattering length density for 300 mV appears higher than the one for 600 mV (contrary to the values given in Table 3) due to the smearing of a thin (15.3 Å) rectangular box with a big roughness parameter (6.3 Å).

The thickness of the SDS organic layer in the form of hemimicelles (at 300 mV) was determined to be 15.3 ± 0.4 Å. The total length of the surfactant is equal to the length of the alkyl tail plus twice the polar headgroup radius and it may be estimated to be 19.8 Å. However, the scattering length density of the SO_4^- polar head is about 3.3×10^{-6} $Å^{-2}$ (calculated from the scattering length density of S and O atoms[26]). In an orientation with the headgroup directed toward the gold surface the difference between this value and the scattering length density of gold (4.6×10^{-6} $Å^{-2}$) is too small for the polar head to contribute to the measured reflectivity of the SDS layer. When the SDS molecule is oriented with the sulfate group toward the solution, the scattering length density of the polar head region should be increased due to the solvation by D_2O molecules. For this orientation, the difference between the SLD for the polar head region and the bulk D_2O (SLD equal to 6.4×10^{-6} $Å^{-2}$) should be small and again the polar head should not contribute significantly to the measured reflectivity. In contrast, the difference between the scattering length densities for the hydrocarbon chain (-0.45×10^{-6} $Å^{-2}$) and the two neighboring phases, gold and D_2O, is large. The SLD of the densely packed hydrocarbon chain was determined by using a cross-sectional area of 20 $Å^2$.[26] Consequently, the main contribution to the observed change in the reflectivity comes from the hydrocarbon tail of the SDS molecule. Therefore, it is safe to say that the thickness determined in neutron reflectivity experiments corresponds to the thickness of the hydrocarbon region rather than to the thickness of the film of SDS molecules. The length of the hydrocarbon tail of the SDS molecule is ~15 Å. Therefore, the thickness of the hydrocarbon region in the hemimicellar film is comparable to the length of the hydrocarbon tail of a fully extended SDS monomer.

It is also possible to evaluate the surface occupancy by the hydrogenated species from the neutron reflectivity

(26) http://rrdjazz.nist.gov/resources/sldcalc.html: site maintained by the NIST Center for Neutron Research.

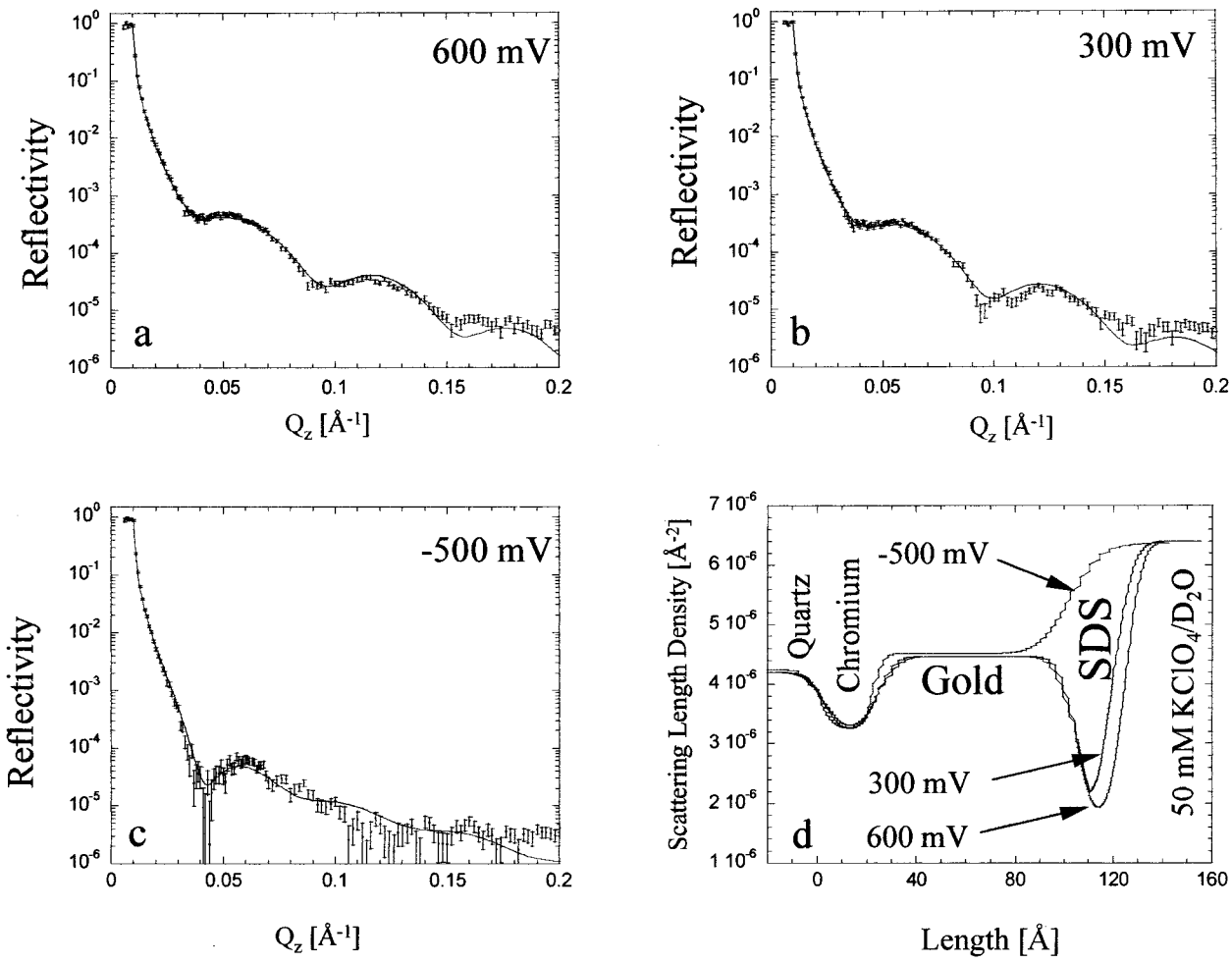

Figure 8. Normalized neutron reflectivity curves for a gold-coated quartz substrate in a 50 mM $KClO_4$/0.3 mM SDS D_2O solution. Reflectivities are shown for three different potentials (vs SCE) applied to the modified quartz electrode: (a) 600 mV, (b) 300 mV, and (c) −500 mV. Panel d shows the scattering length density profiles of the interface as determined from the fitting procedure. The lowest scattering length density for 300 mV appears higher than for 600 mV (contrary to the values given in the Table 3) due to the smearing of a thin (15.3 Å) rectangular box with a big roughness parameter (6.3 Å).

Table 3. Best-fit Parameters for the Modified Quartz Substrate (Working Electrode) in a 0.3 mM SDS/50 mM $KClO_4$ in D_2O Solution[a]

	SDS layer		gold layer		chromium layer			
	scattering length density 10^{-6} Å^{-2}	thickness, Å	scattering length density 10^{-6} Å^{-2}	thickness, Å	scattering length density 10^{-6} Å^{-2}	thickness, Å	roughness σ Å	χ^2
−500 mV			4.465 (fixed)	80.0 (fixed)	3.22 (fixed)	22.0 (fixed)	10.0(1)	3.9
300 mV	1.48(0.1) (72% surface occupancy)	15.3(0.4)	4.465 (fixed)	80.0 (fixed)	3.22 (fixed)	22.0 (fixed)	6.3(0.2)	3.4
600 mV	1.77(0.04) (67% surface occupancy)	20.5(0.6)	4.465 (fixed)	80.0 (fixed)	3.22 (fixed)	22.0 (fixed)	5.2(0.3)	3.4

[a] Scattering length density of the monocrystalline quartz: 4.2×10^{-6} Å^{-2}. Calculated scattering length density of bulk gold: 4.67×10^{-6} Å^{-2}. Calculated scattering length density of bulk chromium: 3.02×10^{-6} Å^{-2}. Calculated scattering length density of the hydrogenated portion of SDS: -0.45×10^{-6} Å^{-2}.

data. Assuming the organic layer only contains solvent and surfactant, the percentage of the surface occupied by dodecyl sulfate can be determined using the following equation

$$\beta_{total} = x\beta_{SDS} + (1 - x)\beta_{D2O} \quad (6)$$

where x is the fraction of surfactant in the film and β_{total}, β_{SDS}, and β_{D2O} are the scattering length densities of the film, surfactant, and solvent, respectively. The value of β_{D2O} is known (6.4×10^{-6} Å^{-2}) and the scattering length density of the hydrocarbon tail of dodecyl sulfate is -0.45×10^{-6} Å^{-2}. This value corresponds to a fully extended, all-trans, hydrocarbon tail of the SDS molecule with a cross-sectional area of 20 Å^2. We assume that the value of β_{SDS} is the same for both states of the adsorbed film.[27] For the hemimicellar film the surface occupancy of the hydrogenated species is 72%. Hence, the film incorporates some quantity of solvent (D_2O).

(27) In fact, $\beta_{SDS} = b/V_{SDS}$ where b is the sum of the scattering lengths of all atoms in the hydrocarbon tail and V_{SDS} the tail molar volume. One may expect that V_{SDS} is larger in the hemimicellar state than it is in the condensed state. However, even if we double V_{SDS} for the hemimicellar state the calculated surface occupancy only increases by an additional 2% (to 74%). For this reason we used the simple approximation of a constant β_{SDS} for both states of adsorption.

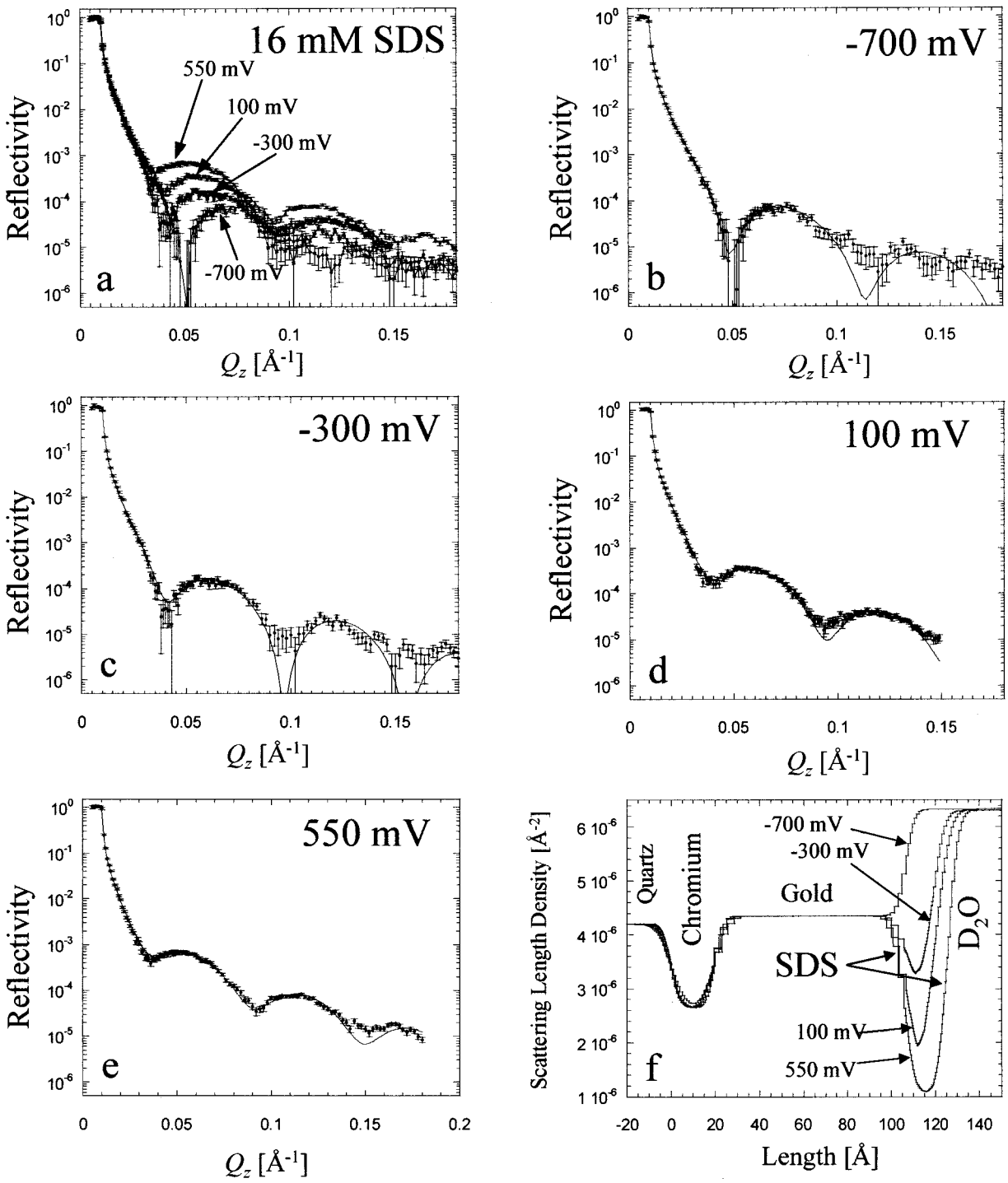

Figure 9. Normalized neutron reflectivity curves for a gold-coated quartz substrate in 16 mM SDS D_2O solution without supporting electrolyte. Panel a shows a progressive change of the reflectivity curves with the applied electrode potential. Panels b−e show individual reflectivity curves and best fits to the reflectivity data. Panel f shows the scattering length density profiles of the interface as determined from the fitting procedure.

At a potential of 600 mV, corresponding to the formation of a condensed film, the thickness of the hydrogenated layer is 20.5 ± 0.6 Å. This value is somewhat larger than the length of the hydrocarbon tail of the SDS molecule; however, it is much lower than the thickness of the hydrocarbon tail region in the bilayer of a dodecyl sulfate molecules, predicted to be ∼30 Å. This result strongly indicates that the film formed at positive electrode polarizations is a monolayer of SDS. The surface occupancy by hydrogenated molecules is only 67% for the condensed film. This is somewhat less than the 74% surface occupancy determined for the hemimicellar state at 300 mV. Therefore, during the phase transition from the hemimicellar to the condensed state the film thickness increases; however, the film either has a higher density of defects or, if it is homogeneous, it contains a larger amount of D_2O. An important piece of information given by the neutron reflectivity data is that the condensed film contains a significant amount of the solvent.

Figure 9 shows the reflectivity curves measured in 16 mM SDS solution in D_2O without supporting electrolyte. These data describe SDS adsorption from a solution with SDS concentration above the cmc point. Panel a in Figure 9 compares the reflectivity curves recorded at different

Table 4. Comparison of the Best Fit Parameters Characterizing the Properties of SDS Film Determined from Neutron Reflectivity Experiments Using Different Electrodes and Different SDS Solutions

solution	potential mV vs SCE	adsorption state	SLD of film, 10^{-6} Å^{-2}	thickness, Å	% occupancy
16 mM SDS	−300	hemimicelles	3.13	13.2	47
16 mM SDS	100	hemimicelles	1.36	13.7	73
16 mM SDS	550	condensed film	1.06	19.8	78
0.5 mM SDS in 50 mM $KClO_4$	100	hemimicelles	1.36	14.0	73
0.5 mM SDS in 50 mM $KClO_4$	600	condensed film	1.70	21.3	68
0.3 mM SDS in 50 mM $KClO_4$	300	hemimicelles	1.48	15.3	72
0.3 mM SDS in 50 mM $KClO_4$	600	condensed film	1.77	20.5	67

electrode potentials. By moving the potential from the negative limit in the positive direction we observe a progressive adsorption of SDS and quite a significant increase of neutron reflectivity from the interface. Panels b to e in Figure 9 show the reflectivity curves recorded for individual potentials and the best fits of a model to these curves. The scattering length density profiles calculated from these fits are shown in panel f of Figure 9 and the parameters characterizing the film properties are summarized in Table 4. Similar experiments were also performed for 0.5 mM SDS solution with 50 mM $KClO_4$ as the supporting electrolyte. These experiments were made using a different chromium and gold-coated crystal. For the SDS film, the scattering length density, film thickness and degree of surface occupancy are listed in Table 4.

The results from different experiments are consistent. For the hemimicellar film the thickness of the hydrogenated layer varies between 13.6 and 15.3 Å. For the condensed film the thickness ranges from 19.8 to 21.3 Å. The data show that there is a small difference between the structure of the film formed at bulk SDS concentrations below and above the cmc point. The surface occupancy by the hydrogenated species is around 75%. This relatively low number may be at least partially due to the defects in film of gold. Alternatively, these data indicate that the film incorporates quite a significant amount of the solvent. A simple estimate shows that this conclusion is consistent with the differential capacity data. The differential capacity may be expressed as

$$C = \frac{\epsilon}{x_2} \tag{7}$$

where ϵ is the permittivity. For the condensed film, one can assume that $x_2 = 20$ Å and that the permittivity is equal to the product of the permittivity of vacuum (8.85 x 10^{-12} C^2 J^{-1} m^{-1}) and square of the refractive index of the hydrogenated layer (∼1.4). These numbers give a value of C (1 μF/cm^2) that is five times smaller than the measured capacity of the condensed film 5 μF/cm^2. The difference between the calculated and experimental values of the differential capacity indicates that the film is much more polar than a compact layer of hydrogenated species and hence must contain a significant amount of the solvent.

Discussion and Conclusions

At this point we can combine the results of the electrochemical data reported herein with our previous scanning probe microscopy studies,[1] to provide a fairly complete picture of SDS adsorption at the Au(111)−solution interface.

The number of SDS molecules per unit cell of the long-range hemimicellar structure is the first important information that we can extract from electrochemical data. The area of the unit cell of the two-dimensional lattice of hemimicellar SDS aggregates can be calculated from the STM images shown in ref 1. It is equal to 206 Å^2. The adsorption isotherm reported in this work indicates that the limiting Gibbs excess for the hemimicellar state is 4.0 $\times$ 10^{-10} mol cm^{-2}. Combination of these data reveals that there are five SDS monomer units per unit cell. This number is smaller than the previous estimate of seven monomer units assumed by us in our earlier paper. The number of seven monomer units was taken from the work of Wanless and Ducker[17b] on the aggregation of SDS on graphite.

The electrochemical data provide useful information concerning the orientation of SDS molecules adsorbed at the electrode surface. For the hemimicellar state, the small shift of the pzc caused by SDS adsorption state indicates that polar heads of SDS molecules are turned toward the solution. The STM images reported in ref 1 suggest that, within the unit cell, two SDS molecules are lying flat at the Au(111) electrode surface. Therefore, we place the three remaining molecules within the unit cell such that their tails are directed toward the metal and the sulfate groups toward the solution.

Another important piece of information provided by electrochemical and neutron reflectivity data concerns the character of the condensed state of the film. AFM and STM images reported in ref 1 clearly indicate that passing through the phase transition results in the formation of a disordered film on the electrode surface. The Gibbs excess data determined in this work show that the surface concentration of SDS is doubled by crossing the phase transition and attains a value of 8.1 $\times$ 10^{-10} mol cm^{-2} in the condensed state. Such an increase of the surface concentration of the surfactant suggests the possibility of bilayer formation. However, neutron reflectivity experiments indicate that the thickness of the condensed film is much less than the length of two fully stretched out SDS molecules and hence is consistent with the thickness of a monolayer rather than a bilayer film. For a monolayer, the surface concentration equal to 8 $\times$ 10^{-10} mol cm^{-2} corresponds to the area per SDS molecule in the film equal to 20.7 Å^2. This number is essentially equal to the cross-sectional area of the hydrocarbon tail of the SDS molecule. It indicates that in the condensed film, the hydrocarbon tails of the SDS molecules are closely packed.

A very high packing density of negatively charged molecules may be accomplished only if the charge of the anionic polar heads is effectively screened by the counter charge on the metal. The charge density data recorded in these studies indicates that a condensed film of SDS forms on the Au(111) surface at positive charge densities close to 40 μC/cm^2. Although, the charge density on the metal is large, it corresponds roughly to half of the negative charge of the SDS molecules in the condensed state equal to $\sigma_1 = zF\Gamma = -77$ μC cm^{-2}. If all SDS molecules in the condensed state were turned with the sulfate group toward the metal, their negative charge would not be effectively screened by the positive charge on the metal and the repulsive forces between the negatively charged polar head groups would disrupt the film. In this case, the energeti-

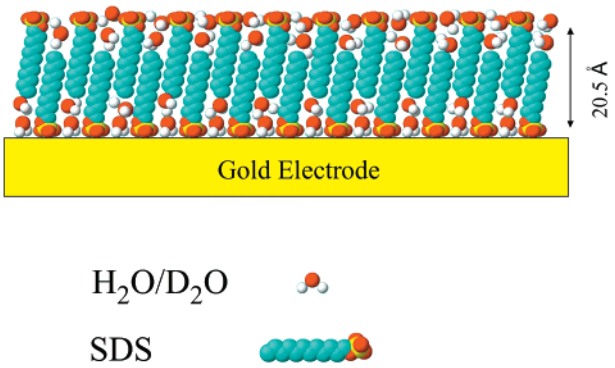

Figure 10. Model of SDS adsorption at the Au(111)−solution interface showing the interdigitated condensed film of SDS molecules formed at positive electrode potentials (large positive charge densities).

cally stable packing of SDS molecules can be accomplished only in an interdigitated film, as shown schematically in Figure 10, in which half of the sulfate groups are turned toward the metal and half toward the solution. The negative charge of the sulfate groups lying on the metal is now effectively screened by the positive charge on the metal of approximately the same absolute magnitude. The charge of the sulfate groups turned to the solution is also screened by the positive counterions from the diffuse part of the double layer. This film is stabilized by van der Waals forces between closely packed hydrocarbon tails. In this model, the thickness of the hydrogenated layer should be somewhat larger than the length of the hydrocarbon tail of the SDS molecule and significantly lower than the thickness of a bilayer, consistent with the neutron reflectivity data.

This model is consistent with the magnitude of the shift of the pzc determined for the condensed state of the film from the charge density data. In this case the value of E_N is determined by the magnitude of the first term in eqs 2 and 3. When SDS molecules are oriented with the polar head toward the metal and hydrocarbon tail toward the solution, to a good approximation $(x_2 - x_1) \approx x_2$. Therefore, the first term of eqs 2 and 3 may be approximated by

$$\frac{zF(x_2 - x_1)}{\epsilon} = \frac{zF\Gamma}{C} \qquad (8)$$

Assuming that in state II all SDS molecules are turned with the polar head to the metal and the hydrocarbon tail to the solution, one gets $(zF\Gamma)/C = -15.4$ V. This number is twice the value of E_N obtained by extrapolation of the charge density data. In contrast, assuming that only half the SDS molecules in the condensed film are turned with their polar heads toward the metal gives the value of $(zF\Gamma)/C = -7.7$ V, in excellent agreement with the experimental result.

In order for the length of the hydrogenated layer to equal 20.5 Å, the SDS molecules oriented in opposing directions have to be shifted from one another as shown in Figure 10. This shift creates a void space that may be filled by solvent molecules, as schematically shown in Figure 10. The void space, created by the shift of the hydrocarbon chains, amounts to about 25% of the volume of the hydrogenated layer. This number is close to the occupancy of the film by solvent calculated from the scattering length density data. The presence of solvent molecules in the film also explains why the differential capacity of the condensed film has such a high value as 5 μF/cm^2.

Finally, strong support for this model comes from the surface force measurements for hemimicellar and condensed states of adsorbed SDS, reported in our previous work.[1] Using AFM, we measured force−distance curves to study the interaction between the negatively charged silicon nitride tip and the SDS covered Au(111) electrode surface. At separations of the tip from the surface comparable to the Debye length, the tip experienced repulsive, double layer forces, described by the exponential function $F = A \exp(-z/k)$ in the regions of both the hemimicellar and condensed films. Compared to the force curves of the hemimicellar state, the forces measured in the condensed film region were characterized by a similar value for the preexponential factor and a somewhat longer decay length k. We were unable to explain these results and we wrote the following statement, "However, an increase of the decay length and a negligible change of the preexponential factor for the curve recorded on the condensed film are difficult to reconcile with the electrochemical data. The charge density data show that for the condensed state the charge of adsorbed surfactant is either compensated or significantly screened by the charge on the metal. In contrast to the experimental result, the preexponential term of the double-layer force should decrease or even become attractive at potentials corresponding to the condensed film. At present, we do not know how to explain this contradiction".[1]

Using the model of the interdigitated surfactant molecules, shown in Figure 10, we can now explain why a repulsive double-layer force is observed at potentials of the condensed film and why the preexponential factor of this force has approximately the same value for the hemimicellar and condensed films. Since the charge of the SDS molecules turned with the polar head toward the Au(111) electrode surface is effectively screened by the charge on the metal, the AFM tip is essentially probing the double-layer force due to the SDS molecules turned with polar heads toward the solution. For an approximately 1:1 ratio of SDS molecules turned up and down, the number of surfactant molecules directed toward the solution is approximately equal to the number of SDS molecules in the hemimicellar state. Therefore, similar electrostatic forces are acting on the AFM tip in the whole range of the electrode potentials. The main difference between the hemimicellar and condensed states is that in the former the force varies periodically in the direction parallel to the surface, reflecting periodicity of the hemimicellar structure, while in the latter the force is uniform across the surface.

The results of this body of work demonstrate the need of a concerted use of multiple techniques to study adsorption and phase transitions in films of surfactants adsorbed at the solid−solution interface. Specifically it shows that electrochemical methods when coupled with additional surface-sensitive techniques, such as SPM and neutron reflectometry, provide unique opportunities to study the different stages involved in the interaction of surfactants with solid surfaces.

Disclaimer. In this paper, any mention of a commercial product does not constitute an endorsement of that product nor does it necessarily mean that this is the best commercial product available.

Acknowledgment. We gratefully acknowledge David Brown from the MST-11 division of the Los Alamos National Laboratory for an excellent job of sputtering gold on the quartz surfaces. The Manuel Lujan Jr., Neutron Scattering Center is a national user facility funded by the

United States Department of Energy, Office of Basic Energy Sciences−Materials Science, under Contract No. W-7405-ENG-36 with the University of California. Our research was supported by a grant from Natural Sciences and Engineering Research Council (NSERC) of Canada. I.B. thanks NSERC for a PGS A scholarship and V.Z. acknowledges the Government of Ontario for an OGS scholarship.

LA001628Q